JCI insight

RESEARCH ARTICLE

Beclin-1 regulates cigarette smoke–induced kidney injury in a murine model of chronic obstructive pulmonary disease

Maria A. Pabón,[1,2] Edwin Patino,[3] Divya Bhatia,[3] Joselyn Rojas-Quintero,[4] Kevin C. Ma,[2] Eli J. Finkelsztein,[1] Juan C. Osorio,[1,2] Faryal Malick,[1] Francesca Polverino,[4] Caroline A. Owen,[4] Stefan W. Ryter,[1] Augustine M.K. Choi,[1,2] Suzanne M. Cloonan,[1] and Mary E. Choi[2,3]

[1]Division of Pulmonary and Critical Care Medicine, Joan and Sanford I. Weill Department of Medicine, Weill Cornell Medicine, New York, New York, USA. [2]NewYork–Presbyterian Hospital, Weill Cornell Medicine, New York, New York, USA. [3]Division of Nephrology and Hypertension, Joan and Sanford I. Weill Department of Medicine, Weill Cornell Medicine, New York, New York, USA [4]Division of Pulmonary and Critical Care Medicine, Department of Medicine, Brigham and Women's Hospital, Harvard Medical School, Boston, Massachusetts, USA.

Chronic obstructive pulmonary disease (COPD), associated with cigarette smoke–induced (CS-induced) emphysema, contributes significantly to the global health care burden of disease. Although chronic kidney disease (CKD) may occur in patients with COPD, the relationship between COPD and CKD remains unclear. Using a murine model of experimental COPD, we show that chronic CS exposure resulted in marked kidney injury and fibrosis, as evidenced by histological and ultrastructural changes, altered macrophage subpopulations, and expression of tissue injury, fibrosis, and oxidative stress markers. CS induced mitochondrial dysfunction, and increased autophagic flux in kidney tissues and in kidney tubular epithelial (HK-2) cells, as determined by LC3B turnover assays. Mice heterozygous for Beclin-1 (*Becn1*$^{+/-}$) were protected from the development of kidney tissue injury and renal fibrosis in response to CS exposure, and displayed impaired basal and inducible mitochondrial turnover by mitophagy. Interestingly, CS caused a reduction of Beclin-1 expression in mouse kidneys and kidney tubular epithelial cells, attributed to increased autophagy-dependent turnover of Beclin-1. These results suggest that Beclin-1 is required for CS-induced kidney injury and that reduced levels of Beclin-1 may confer renoprotection. These results identify the kidney as a target for CS-induced injury in COPD and the Beclin-1–dependent autophagy pathway as a potential therapeutic target in CKD.

Introduction

Chronic obstructive pulmonary disease (COPD), a chronic and debilitating lung disease associated with cigarette smoking, represents the third leading cause of death in the United States (1). COPD is characterized by 3 major disease states: chronic bronchitis or excess mucus production in the larger airways; emphysema or peripheral lung destruction and loss of alveolar attachments; and small airway disease characterized by inflammation and airway remodeling (2, 3). In addition, several subphenotypes of COPD exist, including some that exhibit an accelerated decline in lung function, with frequent exacerbations (4). Systemic components also play a significant role in COPD pathogenesis, such that comorbidities linked to COPD can have a marked effect on individual patient quality of life and prognosis. Specifically, COPD patients have a greater risk of developing cardiovascular disease, lung cancer, infection, and anemia (5, 6). Additionally, emerging studies suggest that the prevalence of chronic kidney disease (CKD) in a subset of COPD patients exceeds that observed in the general population (6, 7). The mechanisms by which COPD patients develop systemic comorbidities remain poorly understood.

CKD, characterized by reduced kidney function or kidney damage that persists for at least 3 months, affects 14% of adults in the United States and represents a significant healthcare burden (8, 9). The pathogenesis of CKD remains incompletely understood but may involve vascular changes, loss of podocytes and renal epithelial cells, extracellular matrix deposition, inflammation, and metabolic dysregulation (10). Successfully identifying and predicting patients at risk for CKD are required to avoid the development

Conflict of interest: The authors have declared that no conflict of interest exists.

Submitted: January 2, 2018
Accepted: August 3, 2018
Published: September 20, 2018

Reference information:
JCI Insight. 2018;3(18):e99592.
https://doi.org/10.1172/jci.insight.99592.

of end-stage renal disease (ESRD) and the subsequent need for renal replacement therapy (11). We have recently shown that structural renal lesions (i.e., injury to glomeruli, renal tubules, and interstitium) occur more frequently in patients with COPD than in control subjects and may be linked to increased endothelial cell damage (12). Despite the possible associations between CKD and COPD, few mechanistic studies to date have linked kidney dysfunction with smoking and/or COPD.

Cigarette smoke (CS) exposure can accelerate the progression of established kidney injury in human and animal models (13–19). Kidney biopsies from patients with a long-standing history of smoking and hypertension exhibit pathologic features of glomerular disease (20). CS exposure remains the most important risk factor for developing COPD (21). The mechanisms mediating CS-induced tissue damage are multifactorial, involving aberrant inflammatory and cellular responses (22), leading to increased oxidative stress, inflammation, and programmed cell death (23, 24). While the above evidence suggests that CS exposure may act as a common pathogenic factor in COPD and CKD, little is known about the role of CS in the etiology of CKD, particularly at the molecular level.

Autophagy is a cellular homeostatic process that degrades and recycles cytoplasmic components, such as damaged organelles or ubiquitinated proteins via their sequestration in double-membraned autophagosomes and subsequent delivery to lysosomes (25). A broad range of signals can activate autophagy, including metabolic processes, environmental stress, infection, and malignancy (26, 27). Execution of the autophagy cascade is mediated by many autophagy-related genes (Atg), including the Bcl-2–interacting protein Beclin-1, which associates with other cellular proteins to form the Beclin-1–interacting complex. In coordination with the Unc-51–like autophagy activating kinase 1 (ULK1) complex, the Beclin-1 complex regulates early events in the initiation of autophagosome formation (21). Another crucial autophagy protein, ubiquitin-like protein microtubule–associated protein 1 light chain 3B (LC3B or ATG8), facilitates autophagosome elongation and maturation, leading to the sequestration of autophagic cargoes (28).

Autophagy has been linked to both beneficial and deleterious effects in disease pathogenesis. We and others have previously demonstrated that autophagy in general, and its mitochondria-specific selective autophagy subtype mitophagy, both play important roles in the response of the lung to CS and, in turn, to the development of COPD (22, 29, 30). Specifically, we have shown that CS activates autophagy and mitophagy in lung tissues from COPD patients, in murine COPD models, and in cell culture systems including lung epithelial cells (22, 29–31). We have also demonstrated that loss of the key autophagy proteins Beclin-1 and LC3B, as well as the mitophagy protein PTEN-induced putative kinase 1 (PINK1), in mouse lungs ameliorates CS-induced lung damage (22, 29–31). In the kidneys, autophagy has been shown to confer cyto- and tissue protection in kidney fibrosis models, including unilateral ureteral obstruction (UUO) (32), sepsis-induced acute kidney injury (33), and diabetic nephropathy (34).

In the current study, we examined the effects of CS exposure on kidney structure and function using an in vivo experimental model of COPD. We evaluated the role of autophagy and mitophagy in kidney tissue of mice exposed to CS, as well as in human renal proximal tubular epithelial (HK-2) cells treated with CS extract (CSE), an established in vitro model of CS exposure. To further examine the role of autophagy in CS-induced kidney injury, we exposed autophagy-deficient Beclin-1–heterozygous (*Becn1*$^{+/-}$) mice to CS for 2 or 6 months. Using this model, we demonstrate that autophagy is regulated in kidneys after CS exposure and that the upstream autophagy effector Beclin-1 regulates CS-induced mitophagy as well as renal injury and fibrosis. Our findings implicate the autophagy pathway in the pathogenesis of CS-induced kidney injury and may lead to the development of new therapeutic approaches for smoking-associated CKD.

Results

CS induces kidney injury in an experimental model of COPD. Chronic whole-body CS exposure in mice is a well-characterized model of experimental COPD. Mice exposed to CS for up to 6 months display airspace enlargement, as evidenced by increases in mean alveolar chord length and airspace diameter, and thickening of the small airways — all established indices of experimental COPD (3, 22, 30, 35). In this study, we sought to determine the effects of chronic CS exposure on the kidney in experimental COPD. Mice exposed to CS for 6 months developed kidney fibrosis as assessed by Masson's trichrome staining (Figure 1A) relative to control mice exposed to room air (RA). Consistently, CS-exposed mice displayed increased collagen deposition in the kidney cortex as determined by Sirius red staining (Figure 1B) and increased fibronectin expression in whole kidney tissue homogenates (Figure 1C and see online supplemental material for uncut gels). Structural changes in the kidney with evidence of diffuse mesangial and glomerular basement

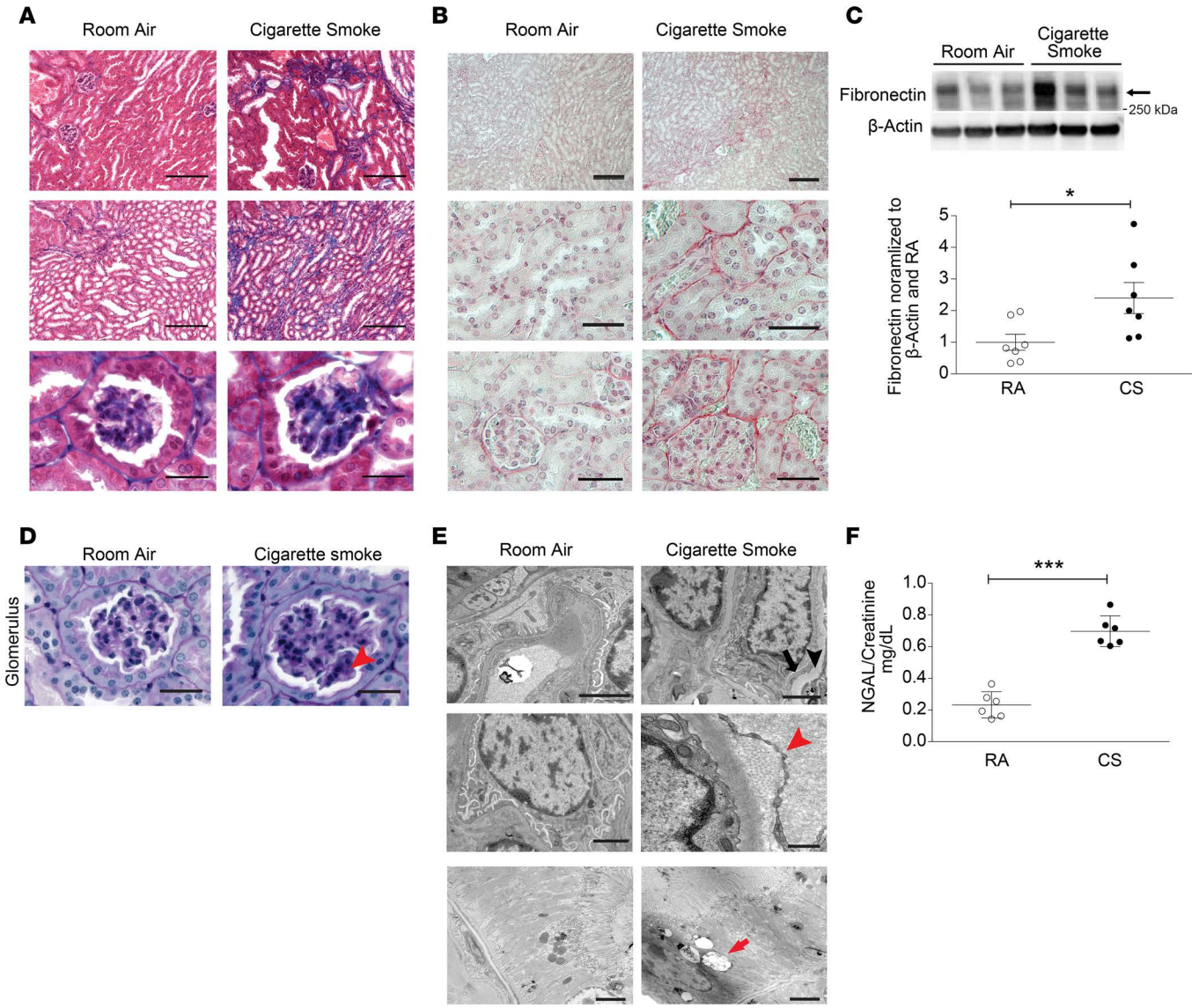

Figure 1. CS induces kidney injury in a murine model of COPD. Kidney sections from mice exposed to room air (RA) or cigarette smoke (CS) for 6 months were stained with (**A**) Masson's trichrome or (**B**) Sirius red. Scale bars: 50 μm and 25 μm (magnified images). (**C**) Western blot for fibronectin expression in kidneys after RA or CS exposure (n = 7 for each group), representative of 3 independent experiments. Graph represents quantification of Western blot data normalized to β-actin and RA control. (**D**) Periodic acid–Schiff (PAS) staining of kidney tissue from mice exposed to CS for 6 months, showing increased glomerular basement matrix content (arrowhead) relative to RA control. Scale bars: 25 μm. (**E**) Transmission electron microscopy (TEM) of kidney sections after 6 months of CS exposure, displaying podocyte foot process effacement (black arrow) and glomerular basement membrane thickening (black arrowhead), interstitial collagen deposition (red arrowhead), and cytoplasmic lipid droplets in tubular cells (red arrow) relative to RA control. Scale bars: 2 μm and 500 nm (collagen deposition in CS group). (**F**) Urine neutrophil gelatinase–associated lipocalin (NGAL) levels quantified by ELISA (mg/dl), normalized to urine creatinine after 6 months of CS exposure (n = 6 per group). All data are mean ± SEM. $^*P < 0.05$, $^{***}P < 0.001$ by 2-tailed Student's t test.

membrane thickening were also evident following 6 months of CS exposure (Figure 1D). Ultrastructural analysis of kidney tissue from CS-exposed mice using transmission electron microscopy (TEM) revealed evidence of podocyte foot process effacement, mild thickening of the glomerular basement membrane, interstitial collagen deposition, and accumulation of cytoplasmic lipid droplets in kidney tubular cells (Figure 1E). Furthermore, mice subjected to chronic CS exposure (6 months) displayed increased urinary levels of neutrophil gelatinase–associated lipocalin 2 (NGAL), a well-characterized kidney injury marker, relative to control mice exposed to RA (36) (Figure 1F). Given that ultrastructural abnormalities were observed in kidney tubular cells of chronic CS-exposed mice, we next evaluated the effect of CS on human proximal tubule kidney cells (HK-2 cells) in vitro. Exposure of HK-2 cells to aqueous CSE, an established model of in vitro CS exposure, dose-dependently decreased cell viability (Supplemental Figure 1; supplemental

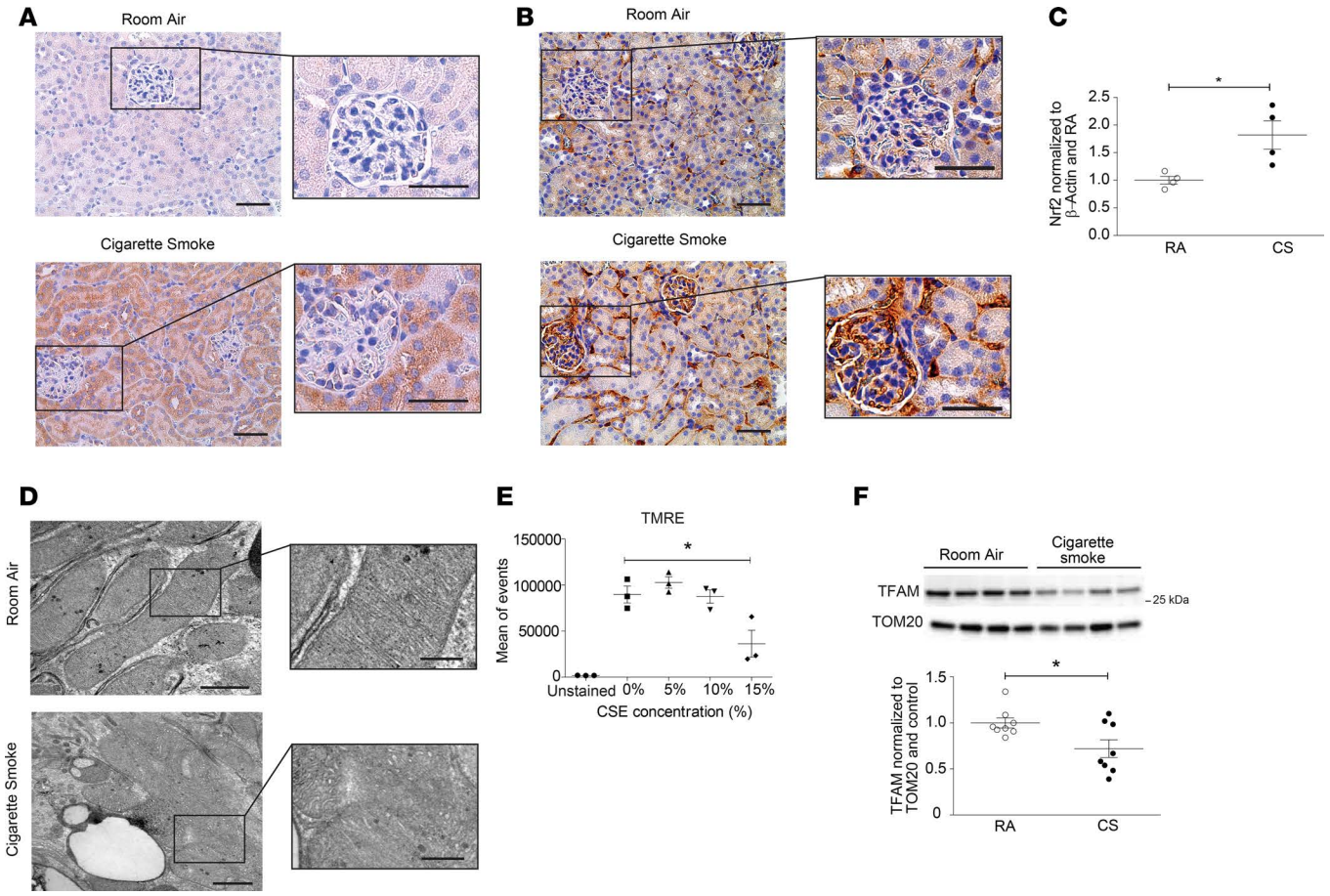

Figure 2. CS induces oxidative stress and mitochondrial injury in a murine model of COPD. (**A**) Nitrotyrosine and (**B**) 8-Oxo-2′-deoxyguanosine (8-oxo-DG) staining detected by immunohistochemical staining of kidney tissue of mice exposed to room air (RA) or cigarette smoke (CS) for 6 months. Scale bars: 50 μm and 25 μm (magnified images). (**C**) Quantification of Nrf2 expression measured by Western blot in kidney tissue from mice exposed to RA or CS for 6 months (n = 4 in each group) normalized to β-actin and control. Data are mean ± SEM. *P < 0.05, analyzed by Student's t test. (**D**) Transmission electron microscopy (TEM) of kidney sections harvested after 6 months of CS exposure, depicting mitochondrial swelling and loss of cristae definition, compared with RA control. Scale bars: 1 μm and 0.5 μm (magnified images). (**E**) Quantification of mitochondrial membrane potential of HK-2 cells treated in vitro with increasing concentrations of CS extract (CSE), measured by tetramethylrhodamine ethyl ester (TMRE) detected by FACS. Data are mean ± SEM. *P < 0.05 by 1-way ANOVA with Bonferroni's post hoc test. (**F**) Representative Western blot of mitochondrial transcription factor A (TFAM) expression in kidneys after 6 months of CS exposure (3 independent determinations), with quantification (n = 8 per group). Data were normalized to TOM20 and RA control. All data are mean ± SEM. *P < 0.05 by 2-tailed Student's t test.

material available online with this article; https://doi.org/10.1172/jci.insight.99592DS1). Taken together, these data confirm that CS can induce kidney injury and fibrosis in a murine model of COPD.

CS induces oxidative stress and mitochondrial injury in an experimental model of COPD. Given that CS is a well-known inducer of oxidative stress (37, 38), we next examined kidney tissues for relative levels of nitrotyrosine and 8-Oxo-2′-deoxyguanosine (8-oxo-DG), two well-characterized markers of oxidative damage, from mice subjected to chronic CS exposure. Nitrotyrosine and 8-oxo-DG formed to a greater extent in the kidneys of CS-exposed mice than in those from RA-exposed control mice (Figure 2, A and B). Additionally, the expression of the nuclear factor (erythroid-derived 2)–like 2 (Nrf-2), an oxidative stress–responsive transcription factor, was also increased in kidney tissue (Figure 2C). Since mitochondria contribute significantly to the production of ROS (39), we also assessed mitochondrial morphology and function in the kidney after chronic exposure to CS. Renal tubular epithelial cells (RTECs) in the kidneys of mice exposed to CS for 6 months exhibited swollen mitochondria, as well as loss of cristae structure and mitochondrial matrix (Figure 2D). Given that complexes of the mitochondrial electron transport chain (ETC) are the major sites of mitochondrial ROS production (40), we assessed the expression of ETC components in response to CS. The expression of mitochondrial ETC complexes III and IV were increased in whole kidney homogenates of mice exposed to CS, with insignificant changes in the expression of complexes I, II, and V (Supplemental Figure 2A). In addition, exposure of

HK-2 cells in vitro to increasing concentrations of CSE resulted in a loss of mitochondrial membrane potential ($-\Delta\Psi_m$) (Figure 2E). Mitochondrial biogenesis is the process by which cells upregulate the expression of nuclear and mitochondrial genes for the de novo generation of mitochondria (41). The expression of mitochondrial transcription factor A (TFAM), a key mitochondrial biogenesis protein, was also decreased in whole tissue lysates of kidneys exposed to CS (Figure 2F). In contrast, no changes in mitochondrial fusion markers (Supplemental Figure 2B) were observed in kidney lysates from mice exposed to CS for 6 months. Taken together, these findings suggest that CS induces mitochondrial stress and increases ROS production in kidney tissue, resulting in oxidative damage to the kidney.

Regulation of autophagy in mouse kidneys after CS exposure. We have previously demonstrated that CS induces the expression and activation of the autophagy protein LC3B in the lungs of mice after CS exposure (22, 29–31). We have also shown that autophagy is induced in RTECs of obstructed kidneys after UUO and can mediate the suppression of kidney fibrosis, suggesting a protective role for this cellular homeostatic process in this specific model of kidney injury (42). Moreover, oxidative stress is a potent inducer of autophagy (43). Here, we observed that kidneys of mice exposed to CS for 6 months displayed an increased abundance of double-membraned autophagosomes in RTECs, as assessed by TEM (Figure 3A). Interestingly, immunohistochemical analysis for Beclin-1 (a major upstream autophagy protein) demonstrated lower Beclin-1 immunostaining in the kidneys of mice exposed to CS for 6 months compared with RA (Figure 3C). The decreased Beclin-1 staining correlated with findings in whole kidney homogenates, where the expression of Beclin-1 was time-dependently reduced in response to CS exposure (1–6 months) (Figure 3, B and D). Similarly, CS reduced the expression of LC3B in kidney tissue, as demonstrated in vivo by immunohistochemical staining (Figure 3F), as well as in whole kidney homogenates in a time-dependent manner (Figure 3, E and G). No changes were observed in the expression of the autophagy proteins Atg7, Atg5, or p62 in whole kidney homogenates after CS exposure (Supplemental Figure 3A). We also examined the expression of markers of programmed cell death pathways, namely apoptosis and necroptosis, in the kidneys of CS-exposed mice (44). After 6 months of CS exposure, there was no significant difference in the kidney expression of pro- or antiapoptotic proteins (i.e., Bax, Bcl-2, cleaved caspase-3) or necroptosis proteins (i.e., receptor-interacting serine/threonine-protein kinase-1 and -3 [RIPK1, RIPK3], and mixed lineage kinase domain–like protein [MLKL]) (Supplemental Figure 3, B–D).

Autophagic activity and turnover of autophagy proteins were increased in kidneys of CS-exposed mice. We have previously reported upregulation of Beclin-1 and LC3B in murine kidneys after UUO, a model of kidney fibrosis (42), whereas in the current study, we observed decline in the kidney expression of LC3B or Beclin-1 after chronic CS exposure. To determine whether the lower levels of autophagy proteins observed in vivo in response to CS were attributable to decreased expression or increased turnover by autophagy, we first assessed LC3B expression in response to CS using an in vivo autophagic flux assay. Flux assays are based on the concept that autophagy is a dynamic process, and that treatment with inhibitors of autophagosome-lysosome fusion/lysosomal acidification (e.g., bafilomycin A1, chloroquine) or inhibitors of lysosome protease activity (e.g., leupeptin) result in the impaired turnover of autophagy substrate proteins, such as LC3B, which can be detected by Western blotting (45) (Figure 4A). In vivo, in the presence of leupeptin, LC3B expression was higher in response to CS when compared with CS in the absence of inhibitor (Figure 4B), suggesting that CS induces an increase in autophagosomal turnover. Similar results were observed with the analysis of autophagic flux in vitro using bafilomycin A1 as the inhibitor. LC3B expression induced by CSE in HK-2 cells was significantly increased in the presence of bafilomycin A1, relative to the absence of bafilomycin A1 (vehicle control) (Figure 4C).

Beclin-1 expression is not known to be regulated by autophagic flux, given that it is not present on mature autophagosomal membranes (46, 47). However, interestingly, we observed that the suppression of Beclin-1 in response to CS was reversed by chemical inhibitors of autophagic flux, as shown in the presence of leupeptin in vivo (Figure 4B) and bafilomycin A1 in vitro (Figure 4C). Similar findings were observed in the presence of the lysosomal inhibitor chloroquine (Supplemental Figure 4A). These data suggest that autophagic activity may negatively regulate Beclin-1 expression in response to CS. Interestingly, livers and hearts from chronic CS-exposed mice did not display changes in Beclin-1 expression after 6 months of CS exposure (Supplemental Figure 4B). Furthermore, in an elastase-induced murine emphysema model, there was no observed difference in Beclin-1 expression in the kidney (Supplemental Figure 4C), suggesting that the downregulation of Beclin-1 expression is a specific response to chronic CS that occurs primarily in the kidney. Taken together, these results suggest that CS increases autophagic flux in kidney tissue in vivo and in tubular epithelial cells in vitro.

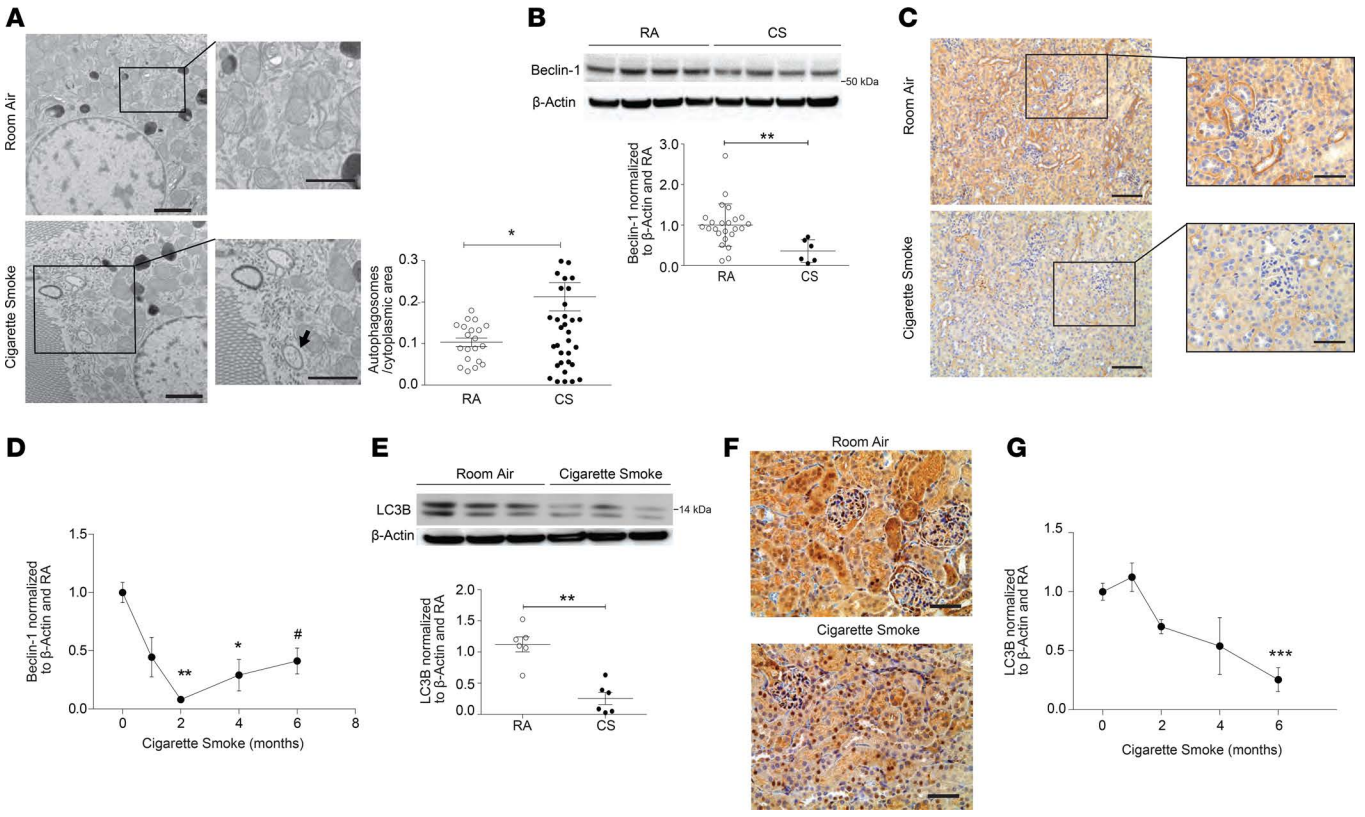

Figure 3. Regulation of autophagy in mouse kidneys after cigarette smoke exposure. (**A**) Representative transmission electron microscopy (TEM) image from kidney tubular cells displaying double-membrane autophagosome formation (black arrow) after 6 months of cigarette smoke (CS) exposure compared with room air (RA) control, with quantification of autophagosomes per cytoplasmic area (mean of autophagosome number in 10 images/group). Scale bars: 2 μm. Data are mean ± SEM. $^{*}P < 0.05$ by 2-tailed Student's *t* test. (**B**) Beclin-1 expression in kidney tissue after 6 months of CS or RA exposure ($n = 24$ for RA, $n = 6$ for CS); representative blot and quantification normalized to β-actin and RA control. Data are mean ± SEM. $^{**}P < 0.01$ by 2-tailed Student's *t* test**.** (**C**) Beclin-1 immunohistochemical staining of kidney tissue sections after 6 months of CS exposure compared with RA. Scale bars: 50 μm and 25 μm (magnified images). (**D**) Beclin-1 expression plotted against time of CS exposure (0 months of exposure, $n = 27$; 1 month of exposure, $n = 6$; 2 months of exposure, $n = 9$; 4 months of exposure, $n = 6$; and 6 months of exposure, $n = 6$). Data are mean ± SEM; $^{*}P < 0.05$, $^{**}P < 0.01$ compared with 0 months of exposure, 1-way ANOVA with Bonferroni's post hoc test; $^{\#}P < 0.05$ compared with 0 months of exposure, 2-tailed Student's *t* test. (**E**) Representative Western blot (3 independent experiments) for LC3B expression in kidneys after 6 months of CS exposure, with quantification ($n = 6$ per group) normalized to β-actin and RA control. Data are mean ± SEM. $^{**}P < 0.01$ by 2-tailed Student's *t* test. (**F**) Immunohistochemical staining for LC3B expression in kidney tissue of mice exposed to CS or RA (6 months). Scale bars: 50 μm. (**G**) Time course of LC3B expression in kidney tissue, and quantification of Western blots from 2, 4, and 6 months exposure to CS, normalized to β-actin and RA control (0 months of exposure, $n = 27$; 1 month of exposure, $n = 6$; 2 months of exposure, $n = 9$; 4 months of exposure, $n = 6$; and 6 months of exposure, $n = 6$). Data are mean ± SEM, $^{***}P < 0.001$ compared with 0 months of exposure, 1-way ANOVA with Bonferroni's post hoc test.

Beclin-1–deficient mice are protected against damage after CS exposure. We have previously reported that *Becn1*$^{+/-}$ mice displayed increased tubular epithelial cell apoptosis in the kidneys after UUO (42). Moreover, *Becn1*$^{+/-}$ mice displayed increased renal fibrosis in the kidneys after UUO, suggesting a protective role of Beclin-1 in the kidney (42). We have also previously described increased collagen deposition in *Becn1*$^{+/-}$ using a kidney fibrosis model (48). *Becn1*$^{+/-}$ mice, which are haploinsufficient, demonstrate reduced autophagy activity as characterized by decreased autophagosome formation and localization of LC3B in autophagosomes (49). Given that an increase in autophagy flux after CS exposure was associated with decreases in Beclin-1 expression, we sought to assess the effects of CS in *Becn1*$^{+/-}$ mice. After 6 months of CS exposure, *Becn1*$^{+/-}$mice were protected from the development of renal fibrosis as measured by Masson's trichrome staining (Figure 5A) and Sirius red staining (Figure 5B) when compared with WT (*Becn1*$^{+/+}$) mice. Additionally, *Becn1*$^{+/-}$mice had lower fibronectin expression in whole kidney homogenates in response to CS (Figure 5C) when compared with *Becn1*$^{+/+}$ mice after CS exposure.

While *Becn1*$^{+/-}$ mice displayed higher oxidative stress levels at baseline, as suggested by increased nitrotyrosine and 8-oxo-DG staining, *Becn1*$^{+/-}$ mice were protected from CS-induced oxidative stress compared with *Becn1*$^{+/+}$ mice (Figure 5, D and E). Urine levels of 8-isoprostane, a marker of oxidative kidney injury, were

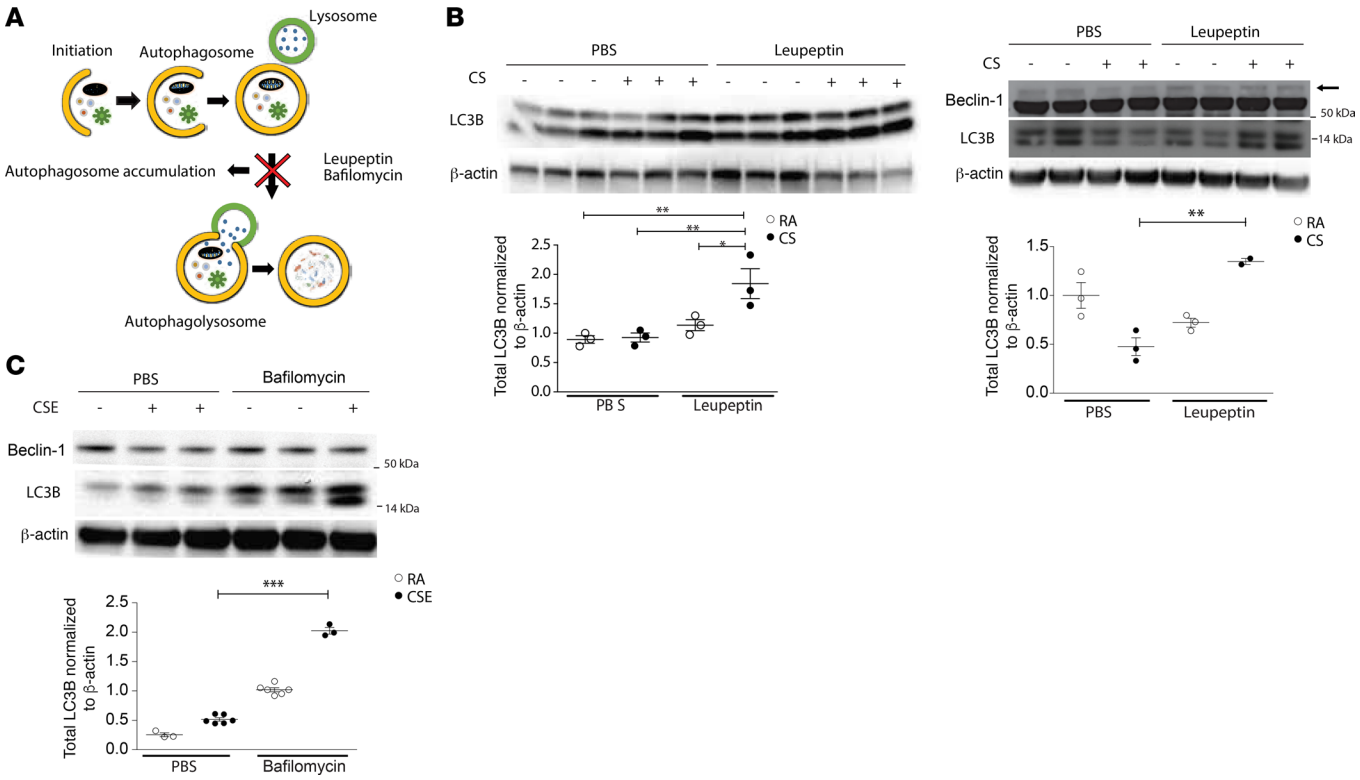

Figure 4. Autophagy activity is induced in mouse kidneys after cigarette smoke exposure. (**A**) Scheme representing autophagic flux experiment in which leupeptin or bafilomycin A1 inhibits autophagosome degradation, leading to autophagosome accumulation. (**B**) Mice subjected to RA or CS for 2 months (left panel) or 6 months (right panel) were assayed for autophagic flux in vivo by injection with leupeptin or vehicle (PBS), followed by Western blotting for LC3B expression in kidney tissue after 2 and 6 months of exposure and Beclin-1 expression after 6 months of exposure. Dot plots represent quantitation of Western blots (n = 3 per group, except for 6 months CS + leupeptin exposure, n = 2 per group). (**C**) HK-2 cells were exposed to CSE in the absence or presence of bafilomycin A1. Representative Western blot of Beclin-1 and LC3B expression to determine autophagic flux in vitro. Dot plots represent quantitation of 3 independent experiments. All data are mean ± SEM.*P < 0.05, **P < 0.01, ***P < 0.001, analyzed by 1-way ANOVA with Bonferroni's post hoc test.

similarly elevated in *Becn1*$^{+/+}$ mice after 6 months of CS relative to air-exposed control mice (Figure 5F), and were lower in *Becn1*$^{+/-}$ mice subjected to CS. Furthermore, urinary NGAL levels did not increase in CS-exposed *Becn1*$^{+/-}$ mice, whereas they were elevated in CS-exposed *Becn1*$^{+/+}$ mice (Figure 5G) relative to corresponding air-exposed control mice. Finally, blood urea nitrogen (BUN) levels were higher after 6 months of CS exposure in *Becn1*$^{+/+}$ mice compared with *Becn1*$^{+/-}$ mice (Figure 5H). These results suggest that Beclin-1 deficiency can protect mice from CS-induced kidney fibrosis and oxidative stress, and that the specific role of Beclin-1 in the pathogenesis of renal fibrosis in response to CS exposure may differ from that in the obstructed kidney.

Beclin-1–deficient mice display an early phenotype of decreased profibrotic macrophages in response to CS exposure. To determine whether there is a specific kidney compartment that is affected by CS at earlier time points, we examined TEM images from kidney tissues of WT mice. After 2 months of CS exposure, there was evidence of podocyte foot process effacement as well as ultrastructural changes indicative of mitochondrial injury, such as swollen mitochondria, in the glomerular compartment (Figure 6A). We also observed increased swelling of the mitochondria in tubular epithelial cells in the kidneys of mice exposed to CS (Figure 6B). The mechanisms mediating CS-induced tissue damage are likely multifactorial, involving aberrant cellular responses. Macrophage infiltration in the kidney is involved in the pathophysiology of kidney diseases, and macrophages are a heterogeneous cell population, characterized by their plasticity and the ability to switch phenotypes in response to different stimuli (50–52). We performed flow cytometry to quantify the different populations of macrophages in the kidney after 2 months of CS exposure. Besides the classic phenotypes (M1, proinflammatory; and M2, profibrotic), infiltrating macrophage populations can be distinguished by quantification of Ly6C expression (52). In the kidney, the different Ly6C populations are related to specific molecular mechanisms; Ly6C-high (participating in injury), Ly6C-intermediate (participating in repair), and

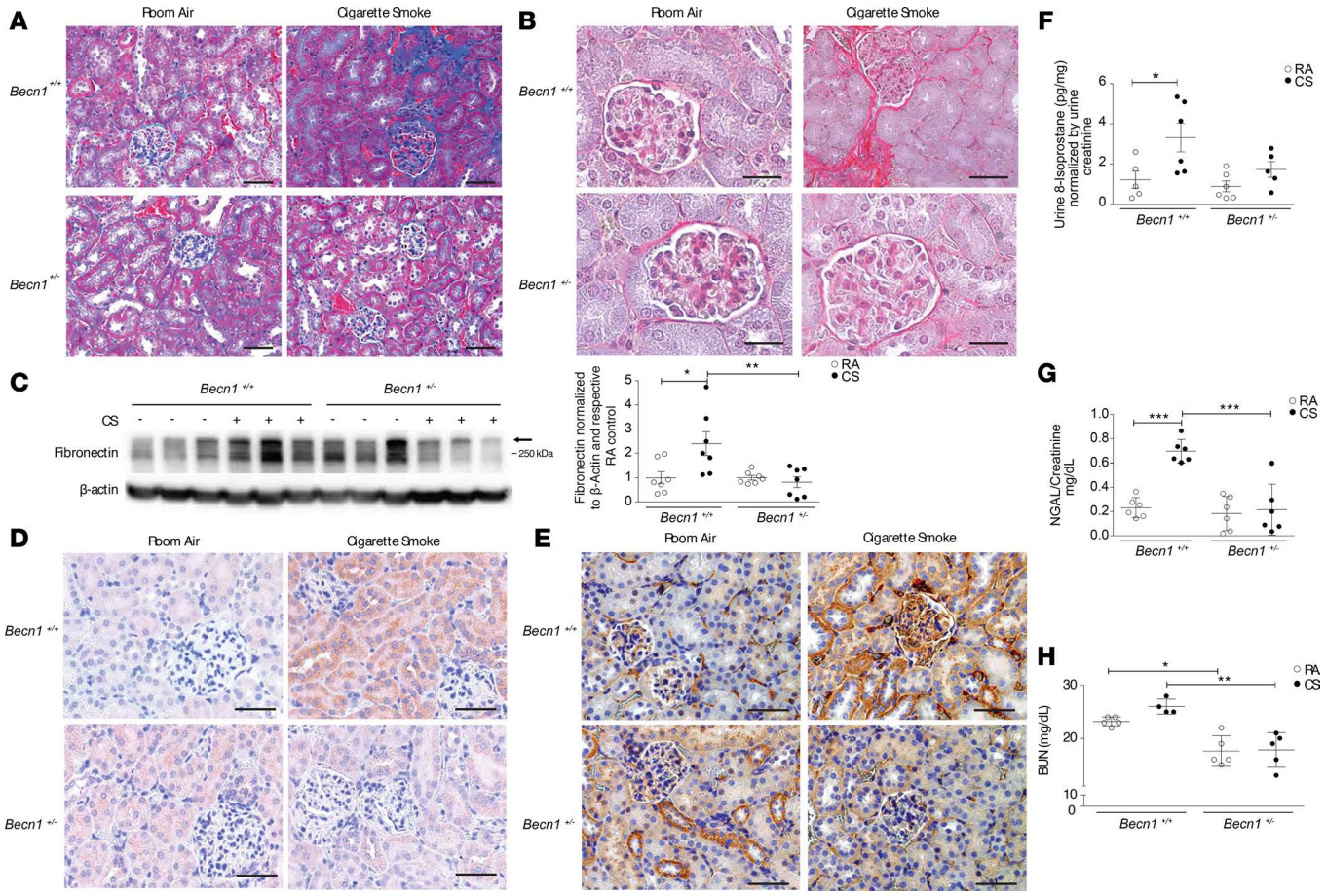

Figure 5. Beclin-1–deficient mice are protected against damage after cigarette smoke exposure. (**A**) Masson's trichrome and (**B**) Sirius red staining of kidney tissue in *Becn1*$^{+/-}$ mice compared with *Becn1*$^{+/+}$ mice after cigarette smoke (CS) exposure. Scale bars: 50 μm (**A**) and 25 μm (**B**). (**C**) Representative blot and quantification showing fibronectin expression in whole kidney tissue homogenates of *Becn1*$^{+/-}$ and *Becn1*$^{+/+}$ mice exposed to CS or room air (RA) for 6 months (n = 7 per group). Data are mean ± SEM. *P < 0.05, **P < 0.01 by 2-tailed Student's t test. (**D**) Nitrotyrosine and (**E**) 8-Oxo-2′-deoxyguanosine (8-oxo-DG) staining detected by immunohistochemistry in *Becn1*$^{+/+}$ mice and *Becn1*$^{+/-}$ after 6 months of CS exposure. Scale bars: 50 μm. (**F**) Urine 8-iso-prostane levels quantified by ELISA (mg/dl), normalized to urine creatinine after 6 months of CS exposure in *Becn1*$^{+/-}$ mice compared with *Becn1*$^{+/+}$ mice (n = 5 for *Becn1*$^{+/+}$ RA and *Becn1*$^{+/-}$ CS mice; and n = 6 for *Becn1*$^{+/+}$ CS and *Becn1*$^{+/-}$ RA mice). (**G**) Urine neutrophil gelatinase–associated lipocalin (NGAL) levels quantified by ELISA (mg/dl), normalized to urine creatinine after 6 months of CS exposure in *Becn1*$^{+/-}$ mice compared with *Becn1*$^{+/+}$ mice (n = 6 per group). (**H**) Blood urea nitrogen (BUN) levels quantified by ELISA (mg/dl), after 6 months of CS exposure in *Becn1*$^{+/-}$ mice compared with *Becn1*$^{+/+}$ mice (n = 5 per group, except *Becn1*$^{+/+}$ CS, n = 4). Data are mean ± SEM. *P < 0.05, **P < 0.01, ***P < 0.001, analyzed by 1-way ANOVA with Bonferroni's post hoc test.

Ly6C-low (participating in fibrosis) (52). Using flow cytometry, we observed increases in the number of proinflammatory (M1 or Ly6c^{hi}) and profibrotic (M2 or CD206^{+}Ly6c^{lo}F4/80^{+}) macrophages in the kidneys of CS-exposed *Becn1*$^{+/+}$ mice (Figure 6, C–E). Importantly, profibrotic macrophages (Figure 6, D and E), but not proinflammatory macrophages (Figure 6C), were significantly lower in *Becn1*$^{+/-}$ mice after 2 months of CS exposure compared with the CS-exposed *Becn1*$^{+/+}$ mice. Our findings indicate that CS induces profibrotic macrophages in the kidney and that Beclin-1 deficiency protects against CS-induced kidney fibrosis.

Beclin-1–deficient mice have decreased mitophagy at baseline that does not increase after CS exposure. In this study, we have demonstrated that CS induces mitochondrial injury in the kidney in response to CS. Upon further analysis using TEM, we observed that RTECs of mice exposed to CS displayed an increased incidence of mitochondrial invaginations (Figure 7A). Such morphological rearrangements may be associated with the selective autophagy of mitochondria (mitophagy), which regulates the degradation and removal of dysfunctional or aged mitochondria (53, 54). We and others have shown that mitophagy is activated in human COPD lung epithelial cells, and in a murine model of experimental COPD (22, 55). Mitophagy contributes to the pathogenesis of experimental COPD via a mechanism involving the activation of the necroptosis pathway and increased epithelial cell death (22). Emerging evidence suggests that mitophagy also plays a crucial role in kidney disease (54). We measured LC3B and markers of mitophagy activity

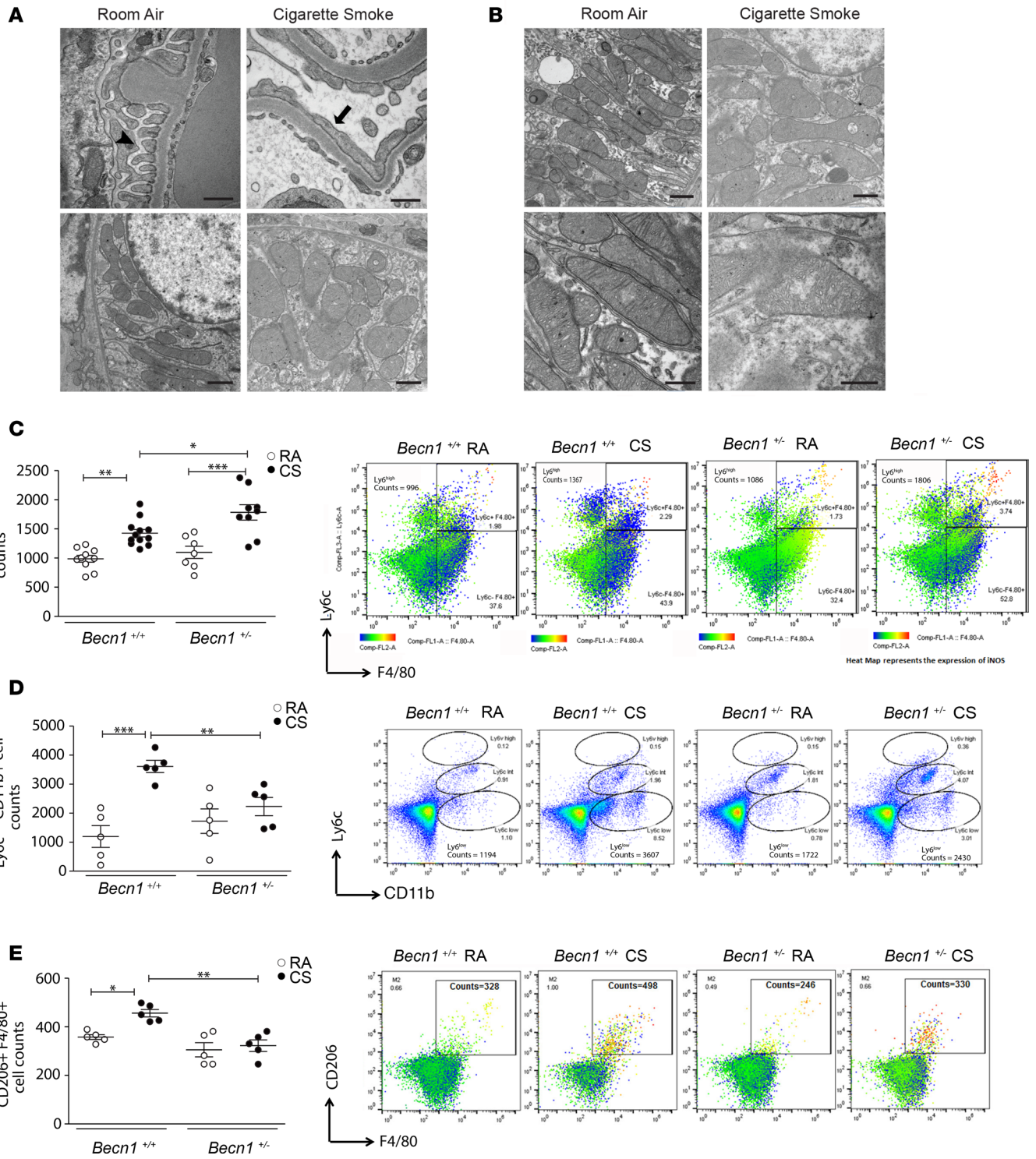

Figure 6. Beclin-1–deficient mice have a decreased profibrotic macrophage phenotype early in the disease process. (**A**) Transmission electron microscopy (TEM) sections of the glomerular compartment after 2 months of cigarette smoke (CS) exposure compared with room air (RA), displaying normal podocyte foot processes in RA control (black arrowhead) and podocyte foot process effacement (black arrow) in CS mice, as well as mitochondrial swelling in CS-exposed mice. Scale bars: 500 nm (upper panels) and 1 μm (lower panels). (**B**) TEM sections of tubular compartment after 2 months of CS exposure compared with RA, displaying mitochondrial swelling in tubular cells in CS-exposed mice. Scale bars: 1 μm (upper panels) and 500 nm (lower panels). (**C**–**E**) Characterization of M1 or proinflammatory (Ly6c^{hi}F4/80^{+}) and M2 or profibrotic (CD206^{+}F4/80^{+}) macrophages performed using flow cytometry, with evidence of (**C**) an increased Ly6C^{hi} iNOS-expressing population in *Becn1*$^{+/-}$ compared with *Becn1*$^{+/+}$ mice (n = 10 for *Becn1*$^{+/+}$ RA, n = 12 for *Becn1*$^{+/+}$ CS, n = 7 for *Becn1*$^{+/-}$ RA, n=9 for *Becn1*$^{+/+}$ CS), but (**D** and **E**) decreased infiltration of CD206^{+}F4/80^{+} and Ly6C^{lo} populations in *Becn1*$^{+/-}$ compared with *Becn1*$^{+/+}$ mice (n = 5 per group) after 2 months of CS exposure. All data are mean ± SEM. *P < 0.05, **P < 0.01, ***P < 0.001, analyzed by 1-way ANOVA with Bonferroni's post hoc test.

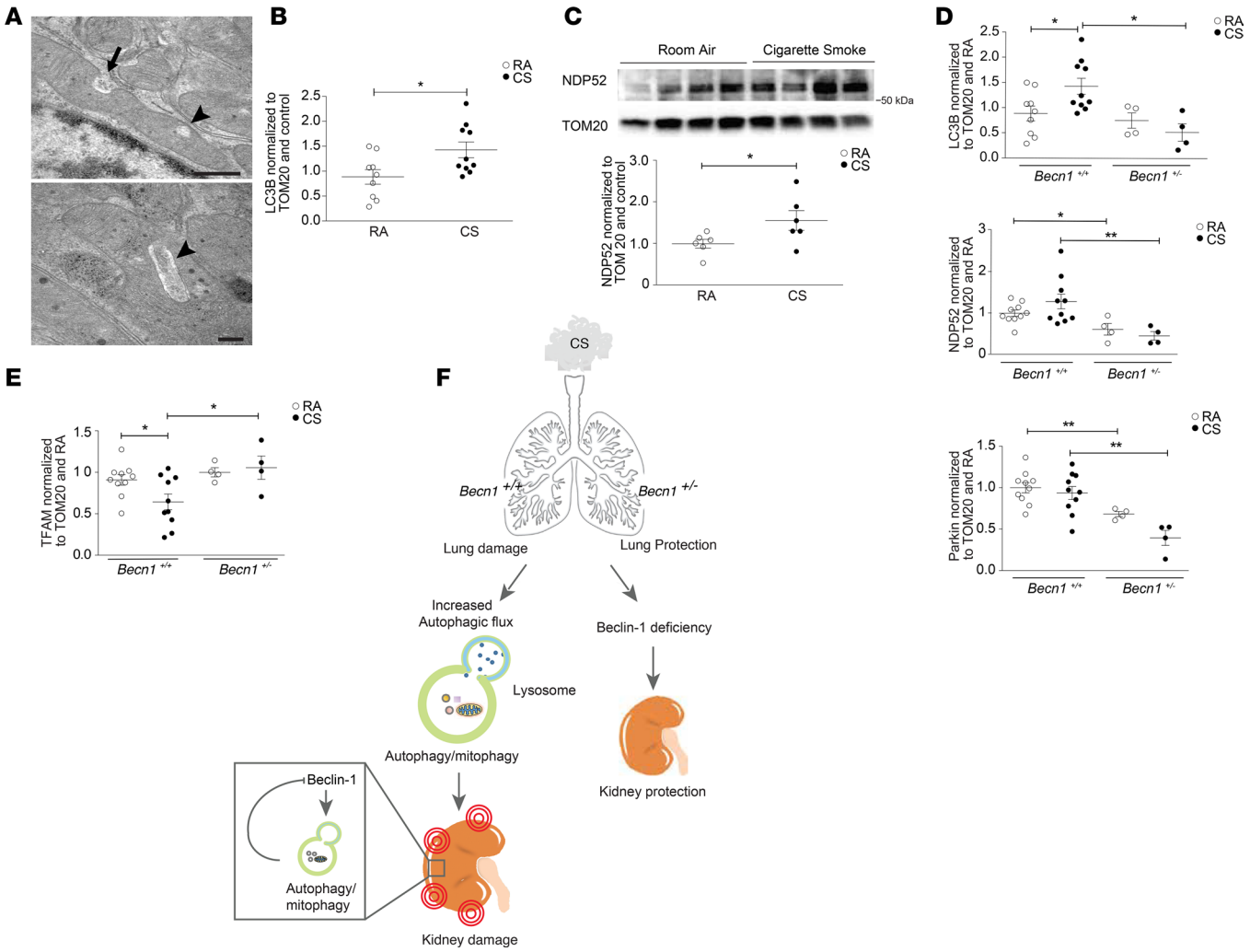

Figure 7. *Becn1*$^{+/-}$ mice have decreased mitophagy at baseline that does not increase after cigarette smoke exposure. (**A**) Mitochondria of renal tubular epithelial cells of WT mice exposed to cigarette smoke (CS), showing invaginations (arrow) and loss of mitochondrial matrix (arrowhead) relative to RA control. Scale bars: 500 nm (top) and 200 nm (bottom). (**B**) Quantification of LC3B detected in mitochondrial fractions from WT mice, normalized to TOM20 and room air (RA) control (n = 9 for RA, n =10 for CS). (**C**) Representative Western blot of NDP52 in mitochondrial fractions from WT mice exposed to 6 months of CS compared with RA. Graph represents quantification of Western data normalized to TOM20 and RA control (n = 9 for RA, n = 10 for CS). (**D**) Quantification of Western blots of LC3B, NDP52, Parkin and (**E**) Mitochondrial transcription factor A (TFAM) expression detected in mitochondrial fractions after 6 months of CS or RA exposure in *Becn1*$^{+/-}$ mice relative to *Becn1*$^{+/+}$ mice. Data were normalized to TOM20 and control (n = 10/group for *Becn1*$^{+/+}$ mice, and n = 4/group for *Becn1*$^{+/-}$ mice). All data are mean ± SEM. *P < 0.05, **P < 0.01, analyzed by Student's t test (**B** and **C**) and 1-way ANOVA with Bonferroni's post hoc test (**D** and **E**). (**F**) Diagram representing CS-induced kidney injury. After systemic exposure to CS, autophagy is upregulated in kidneys in association with kidney injury. *Becn1*$^{+/-}$ mice have reduced autophagy and display reduced kidney injury after CS exposure. The increased autophagic activity and autophagosome turnover in response to CS exposure reduces Beclin-1 steady-state levels, as a potential compensatory mechanism.

in mitochondrial fractions isolated from the kidneys of CS-exposed mice. The expression levels of LC3B as well as calcium-binding and coiled-coil domain–containing protein 2 (NDP52) were increased after CS exposure (Figure 7, B and C). NDP52 is a recently described outer-membrane mitochondria receptor with LC3-interacting regions that can mediate parkin-independent mitophagy (56) (Supplemental Figure 5A). The expression of other mitophagy-related proteins, such as parkin and optineurin (OPTN), were not altered by CS exposure (Supplemental Figure 5B).

Next, we assessed mitophagy activity in *Becn1*$^{+/-}$ mice after 6-month exposure to CS. LC3B and NDP52 expression levels in mitochondrial fractions isolated from *Becn1*$^{+/-}$ kidney tissue after CS exposure, were significantly lower when compared with those of mitochondrial fractions isolated from WT *Becn1*$^{+/+}$ kidney tissues recovered from mice subjected to chronic CS (Figure 7D). Parkin expression in the kidney was lower in the *Becn1*$^{+/-}$ mice at baseline, when compared with WT mice, and was further decreased after CS exposure (Figure 7D). This suggests that *Becn1*$^{+/-}$ mice display reduced activation of mitophagy in the kidney in

response to CS exposure. Furthermore, TFAM expression was not affected after CS exposure in *Becn1*$^{+/-}$ mice compared with *Becn1*$^{+/+}$ mice (Figure 7E), suggesting a preserved capacity for mitochondrial replication.

Discussion

A potential association between COPD and CKD prevalence has previously been suggested in several studies (6, 12). COPD patients may exhibit an increased risk of lower estimated glomerular filtration rate (eGFR) (12), higher serum NGAL levels (57–59), and greater microalbuminuria (12, 60–62). Microalbuminuria has also been associated with a greater prevalence of hypoxemia (60), all-cause mortality (62), and acute exacerbations (63) in COPD patients. Additionally, lower eGFRs have been associated with lower lung function (i.e., forced expiratory volume in 1 second [FEV_1]) (12), as well as increased severity of emphysema in current and former smokers (64). Additionally, "healthy smokers" without COPD may display signs of abnormal renal function (65), along with pathologic features of glomerular disease (20). Although these observations suggest that the prevalence of renal damage in COPD may be associated with smoking status, a mechanistic link associating CKD with CS-induced COPD remains unclear.

In the present study, we demonstrate that chronic exposure to CS induces kidney injury, as demonstrated by renal fibrosis and elevated BUN and urine NGAL levels in a murine model of CS-induced COPD. We also link CS-induced renal damage with increases in oxidative stress markers, including elevated nitrotyrosine (a marker of protein tyrosine oxidation), 8-oxo-DG (a marker of DNA oxidation), and urinary 8-isoprostane, as well as increases in the expression of Nrf-2 in murine kidneys exposed to CS for 6 months. These observations are consistent with our previous findings that CS exposure results in higher levels of advanced glycation end products (AGEs) and receptor of advanced glycation end products (RAGEs) in glomerular endothelial cells of murine kidneys (12). We also detected evidence of mitochondrial dysfunction in kidney cells in vivo and in vitro upon CS exposure. These results are aligned with the fact that the kidneys are rich in mitochondria (66), and that CS has multiple chemical components that can increase the production of ROS in kidney endothelial (67) and mesangial cells (18), as well as inducing mitochondrial dysfunction in lung epithelial and skeletal muscle cells (22, 68–72).

ROS have been shown to induce autophagy (43). Moreover, autophagy proteins such as p62 have been shown to contribute to the regulation of antioxidant signaling pathways including the Keap1-Nrf2 system (73). Consistently, we demonstrate for the first time to our knowledge that autophagy is regulated in kidney cells in vivo and in vitro upon CS exposure. Specifically, we show increased autophagosome formation and LC3B turnover in response to CS and suggest that autophagy may be activated by CS-associated ROS production. In this study, we also demonstrate increases in LC3B and NDP52 expression in mitochondrial fractions of kidney homogenates isolated from mice exposed to CS, as well as the increased appearance of mitochondrial invaginations by TEM. These data suggest that CS activates mitophagy in murine kidneys, which correlates with our previous observations of enhanced mitophagy in murine lungs exposed to CS (22). Consistently, TFAM, a key mitochondrial biogenesis protein that regulates the transcription of the mitochondrial genome, is decreased in kidney tissue after CS exposure. Mitochondrial homeostasis is dependent on a fine balance of mitophagy and mitochondrial biogenesis. Increasing evidence suggests that mitophagy may have important roles in the pathogenesis of kidney diseases (74, 75). Mitophagy is crucial to maintaining functional mitochondria, especially in the context of oxidative stress (76). Given that parkin levels were not regulated by CS, we suggest that CS-induced mitophagy in the kidney may represent NDP52-driven, parkin-independent mitophagy, whereby PINK1 can recruit NDP52 and/or OPTN to the mitochondria, promoting mitochondrial ubiquitination and autophagosomal degradation (56). Further studies will be required to evaluate the precise mechanism of CS-induced mitophagy in CS-induced kidney damage.

Our studies show that chronic CS exposure causes a decline in Beclin-1 and LC3B protein levels. This apparent decline appears to be due to increased autophagic activity, rather than inhibition of de novo expression, as evidenced by the autophagy flux assays demonstrating that Beclin-1 protein levels are restored with the application of autophagy inhibitors such as bafilomycin. Similarly, LC3B steady-state levels decline in response to upregulated autophagy during CS exposure, and these also can be restored with the application of autophagy inhibitors. Hence, CS exposure increases autophagosomal turnover, and this increase in autophagic activity drives the decline of Beclin-1; this highlights the presence of a possible negative feedback loop between autophagy activation and Beclin-1 expression in kidney cells, which, to our knowledge, has yet to be described. This process may represent a defense mechanism, given that Beclin-1 deficiency is associated with protection from CS-induced kidney injury (Figure 7F). Further studies are

needed to confirm whether such a reduction in Beclin-1 protein levels in response to increased autophagy occurs as a negative feedback regulatory mechanism to attenuate autophagy, or whether lysosomal inhibition also plays a role. This is a finding that we have not observed previously in vitro and in vivo in the lungs, where Beclin-1 expression levels were relatively stable after CS exposure, or in other organs of mice exposed to CS.

The notion that a reduction in Beclin-1 may be renoprotective is supported by our studies using autophagy-deficient Beclin-1–heterozygous mice. We demonstrate that genetic deficiency of Beclin-1 confers protection against CS-induced kidney injury in vivo. Specifically, we show that *Becn1*$^{+/-}$ mice have decreased fibrosis, reduced oxidative stress, reduced BUN, and lower urinary NGAL and urinary 8-isoprostane levels in response to CS compared with *Becn1*$^{+/+}$ mice. We also provide evidence for lower profibrotic macrophage numbers in the *Becn1*$^{+/-}$ mice after 2 months of CS exposure, which suggests that *Becn1*$^{+/-}$ mice exhibit an antifibrotic phenotype early in the disease process.

These experiments further suggest that Beclin-1 haplodeficiency, leading to lower basal autophagy or reduced capacity for Beclin-1–dependent initiation of autophagy in response to CS, provides renoprotection. These observations, taken together, suggest that Beclin-1 contributes to renal pathology in the CS exposure model, as we had demonstrated similar findings in the lung wherein Beclin-1 also worsened CS-induced lung tissue injury (29). We have previously reported that *Becn1*$^{+/-}$ mice displayed increased renal fibrosis in the kidneys after UUO relative to *Becn1*$^{+/+}$ mice, suggesting a protective role of Beclin-1 in the obstructed kidney (42). Thus, the results obtained in the CS-induced kidney injury model differ from our previous findings in the obstructed kidney, suggesting that there may be disease-specific mechanisms and that different types of kidney injury trigger distinct context-specific responses.

In this study we suggest a potential role for Beclin-1 in the regulation of mitophagy in renal disease progression during CS-induced injury. Loss of Beclin-1 inhibits CS-induced mitophagy in the kidney, as determined by lower levels of LC3B, parkin, and NDP52 in mitochondrial fractions from *Becn1*$^{+/-}$ compared with WT mice after CS exposure. Previous studies have proposed a role for Beclin-1 in the initiation of mitophagy, by its interaction with parkin, with Beclin-1 depletion inhibiting parkin translocation to mitochondria (77). Based on our observations, Beclin-1 depletion may provoke a decrease in mitophagy as a protective response to limit CS-induced kidney damage. Interestingly, we have also demonstrated in the lung that mitophagy is associated with worsened CS-induced lung tissue injury (22). Further studies are required to investigate the role of Beclin-1 in parkin-independent mitophagy and mitochondrial dynamics. In our study, we cannot exclude the possibility that Beclin-1 may have other autophagy/mitophagy-independent roles that contribute to the responses of the kidney to CS exposure, and which may be partially influencing the protective effects observed with Beclin-1 depletion. Interestingly, we did not observe significant differences in apoptosis or necroptosis markers after CS exposure in the kidneys. This observation contrasts our previous observations in the lungs, where autophagy induces extrinsic apoptosis (30) and necroptosis (22), leading to lung epithelial cell death. Future studies investigating the different cell death modalities that are potentially activated in CS-induced CKD are warranted.

In summary, our data demonstrate that autophagy is increased in murine kidneys upon CS exposure, most likely as a response to increased oxidative stress and mitochondrial dysfunction. We demonstrate that Beclin-1–haplodeficient mice are protected from renal injury induced by CS. These findings suggest that the baseline expression of Beclin-1 is required for promoting the pathogenic process leading to kidney fibrosis that may require Beclin-1 for initiation of autophagy. We have shown that progressive increases in autophagy activity during CS exposure are associated with fibrotic changes in tissue. These increases in autophagy activity also promote increased consumption of autophagy substrate proteins, among which we have identified Beclin-1 itself as a target. We conclude that genetic deletion of Beclin-1 is protective specifically in the CS-induced kidney injury model and not in alternate models of kidney fibrosis such as UUO. Furthermore, we predict that depletion of Beclin-1 by autophagosomal turnover is also protective. Autophagy induction is commonly regarded to occur initially in tissues as a defense mechanism, to preserve tissue function and clear damaged organelles and proteins (78). Despite the cytoprotective effects observed in many model systems, autophagy can also be associated with tissue injury (79). These examples illustrate that the outcome of autophagy activation can be adaptive or maladaptive, and vary with specific model, cell type, or disease context. We believe that the autophagic turnover of Beclin-1 observed in the current study represents a counterregulatory mechanism to limit excessive autophagy activation. The equilibrium between autophagic activity and Beclin-1 expression may be a critical determinant in the development of CS-induced kidney injury.

These findings suggest a novel intracellular mechanism for regulating CS-induced kidney injury by autophagy that may lead to the development of therapies to prevent renal damage.

Methods

Animals. *Becn1*$^{+/-}$ mice were obtained from Beth Levine (University of Texas Southwestern Medical Center at Dallas, Dallas, Texas, USA). WT C57BL/6 littermates mice were used as controls.

In vivo CS exposure and chemical treatments. Age- and sex-matched mice (6–12 weeks of age) were exposed to RA or CS in whole-body exposure chambers for 2 hours per day (150 mg/m^3), 5 days per week, for 6 months. At the end of the exposure regimen, both kidneys were isolated. The left kidney was divided in half. One half was fixed in 4% formalin for TEM, and the other half was fixated for paraffin blocks. The right kidney was flash-frozen in liquid nitrogen and stored at –80°C for protein quantification.

Cell culture and CSE treatment. Human HK-2 kidney tubular cells were maintained in Dulbecco's Modified Eagle Medium: Nutrient Mixture F-12 (DMEM/F12, Thermo Fisher Scientific) supplemented with 10% FBS and 1% penicillin-streptomycin. CSE was prepared and added to culture media as previously described (22, 29).

In vivo autophagic flux assay. The in vivo autophagic flux assay was performed as described previously (45). Mice exposed to CS or RA were given an intraperitoneal injection of 40 mg/kg leupeptin (MilliporeSigma) in saline 1 hour or 24 hours following the final CS treatment. Control mice received an equal volume of the vehicle. Kidney tissues from the leupeptin-treated RA and CS mice were harvested 2 hours later. The tissues were flash-frozen, and LC3B turnover was assessed in the lysosome-enriched (LE) fraction. To quantify the LC3B levels, we performed Western blot analysis. Autophagic flux was defined as the difference in LC3B quantity on Western blots obtained in the presence and absence of the inhibitor (leupeptin).

In vitro autophagic flux assay. HK-2 cells were exposed to 10% CSE for 12 hours and then treated with 25 μM chloroquine (CQ) or bafilomycin (BAF) for 2 hours before harvesting. Control cells were treated with CQ or BAF in the absence of CSE treatment. Cell lysates were then analyzed by standard immunoblot assays for LC3B expression. Autophagic flux was defined as the difference in LC3B quantity (densitometer units) on Western blots obtained in the presence and absence of the inhibitor (CQ or BAF).

Sample preparation for Western immunoblot assay and ELISA. Kidney tissue was homogenized in Tissue Extraction Reagent I (Life Technologies, FNN0071). A mitochondria-enriched fraction was obtained from kidney specimens using the Mitochondria Isolation Kit (MITOISO1, Sigma-Aldrich) according to the manufacturer's protocol. Cell culture lysates were prepared using 1× RIPA buffer. Lysates were boiled for 10 minutes in NuPAGE sample loading buffer (Invitrogen). Proteins were separated by electrophoresis through NuPAGE 4%–12% Bis-Tris gels (Invitrogen) and transferred onto a nitrocellulose blotting membrane (Amersham Protran Premium 0.2) by electroblotting. Membranes were incubated with the following anti-mouse primary antibodies and concentrations: Beclin (Santa Cruz Biotechnology Inc., sc-11427, 1:2,000), LC3B (MilliporeSigma, L7543, 1:2,000), collagen I (Abcam, ab21286, 1:1,000), fibronectin (Abcam, ab2413, 1:1,000), Nrf2 (Cell Signaling Technology, 12721, 1:1,000), Keap1 (Cell Signaling Technology, 4617, 1:1,000), OXPHOS (Abcam, ab110413, 1:1,000), TFAM (Abcam, ab131607, 1:1,000), NDP52 (Novus, H00010241-B01P, 1:1,000), OPTN (Abcam, ab23666, 1:1,000), MFN1 (Abcam, ab57602, 1:1,000), OPA1 (GeneTex, GTX48589, 1:1,000), MFN2 (Cell Signaling Technology, 9482, 1:1,000), TOM20 (Santa Cruz Biotechnology Inc., sc-11415, 1:1,000), followed by an HRP-conjugated secondary antibody (1:2,500; Santa Cruz Biotechnology Inc.). HRP activity was detected by chemiluminescence with SuperSignal West Pico Luminol Enhancer Solution (Thermo Fisher Scientific). Membranes were then stripped and reprobed with anti–mouse actin antibody (1:1,000) as a loading control. Immunoblot analysis was done using NIH ImageJ.

Blood and urine samples. BUN and urine creatinine were measured using a Beckman Coulter AU 680 chemistry analyzer. 8-Isoprostane was quantified in the urine using an ELISA kit according the manufacturer's instructions (Abcam, 175819). Lipocalin-2 (NGAL) quantification in the urine was performed using the Mouse Lipocalin-2/NGAL immunoassay by R&D Systems (MLCN20).

Immunohistochemical staining. Formalin-fixed, paraffin-embedded, 5-μm-thick kidney sections were prepared. To perform immunohistochemical analysis, paraffin-embedded tissues were deparaffinized in xylene, rehydrated, and retrieved by target retrieval solution 10× (Dako, s1699) for 45 minutes. Tissues were immunostained with rabbit antibody against mouse nitrotyrosine (EMD Millipore, AB5532), mouse antibody against mouse 8-oxoguanine (8-oxoG) (EMD Millipore, MAB3560), rabbit antibody against mouse Beclin-1 (Santa Cruz Biotechnology Inc., sc-11427), rabbit antibody against mouse LC3B (Cell Signaling Technology, 2775),

using a VECTASTAIN Elite ABC Kit (PK-6101; Vector Laboratories) according to the manufacturer's protocol. Images were captured using an EVOS FL Auto microscope (Invitrogen, Thermo Fisher Scientific).

TEM. Kidney specimens were washed with serum-free media or appropriate buffer then fixed with a modified Karnovsky's fixative of 2.5% glutaraldehyde, 4% paraformaldehyde, and 0.02% picric acid in 0.1 M sodium cacodylate buffer at pH 7.2. Following a secondary fixation in 1% osmium tetroxide, 1.5% potassium ferricyanide samples were dehydrated through a graded ethanol series and embedded in an EPON analog resin. Ultrathin sections were cut using a DiATOME diamond knife on a Leica Ultractut S ultramicrotome. Sections were collected on copper grids and further contrasted with lead citrate and viewed on a JEM 1400 electron microscope (JEOL) operated at 120 kV. Images were recorded with a VELETA 2K × 2K digital camera (Olympus-SIS).

Cell viability. Cytotoxicity was assessed by the alamarBlue assay (Thermo Fisher Scientific, DAL1025) after CSE exposure at various concentrations for 24 hours according to the manufacturer's instructions.

Determination of mitochondrial membrane potential by flow cytometry. Cells were incubated with CSE at various concentrations for 16 hours, and mitochondrial membrane potential was measured by tetramethylrhodamine ethyl ester (TMRE) using the Mitochondrial Membrane Potential Assay Kit (Abcam, ab113852) for 30 minutes. Cells were trypsinized, and fluorescence was measured using a BD Accuri C6 Flow Cytometer. Results were analyzed using FlowJo software version 10.8 (TreeStar Inc.).

Characterization of macrophage population by multicolor flow cytometry. Characterization of M1 or proinflammatory ($Ly6c^{hi}F4/80^{+}$) and M2 or profibrotic ($CD206^{+}F4/80^{+}$) macrophages were performed using flow cytometry. Briefly, a single-cell suspension was obtained by digesting freshly isolated kidney tissues with 2 mg/ml collagenase type I (Gibco, Invitrogen) for 30 minutes at 37°C. Isolated cells were washed twice in FACS buffer (PBS with 2% FBS and 2 mM EDTA, Gibco, Invitrogen). The nonspecific sites were blocked by incubating cells with anti CD16/32 antibody (BioLegend) for 15 minutes at 4°C. Cells were stained with anti-Ly6c, anti-CD11b, anti-CD206, anti-F4.80, and anti-iNOS antibodies. The fixation permeabilization treatment was performed for intracellular staining with anti-iNOS antibody. The incubations with antibody cocktails were performed for 40 minutes at 4°C in the dark. All antibodies and permeabilization buffer were procured from Thermo Fisher Scientific. Finally, the stained cells were washed twice with FACS buffer and fixed with 2% paraformaldehyde (Santa Cruz Biotechnology Inc.). The cells were captured (50,000 events per sample) using BD Accuri C6 (BD Biosciences), and the data were analyzed using FlowJo version 10.8.

Statistics. Statistical analysis was conducted using Prism 5.0 (GraphPad Software). Data are presented as mean ± SEM from at least 3 independent experiments. Differences in measured variables between experimental and control groups were assessed using the Student's *t* test and between multiple groups and conditions using 1-way and 2-way ANOVA and Bonferroni's post test. *P* values were calculated, and minimum statistical significance was accepted at $P<0.05$.

Study approval. All animal experimental protocols were approved by the IACUC at Weill Cornell Medicine and the Harvard Standing Committee for Animal Welfare at Harvard Medical School, Brigham and Women's Hospital.

Author contributions

MAP, SMC, AMKC, and MEC conceived and designed the study. MAP, EP, DB, JQ, KCM, JCO, FM, FP, EJF, and CAO performed experiments. SMC, SWR, AMKC, and MEC provided critical analysis and discussions. MAP, SMC, SWR, AMKC, and MEC wrote the manuscript. All co-authors reviewed and approved the final manuscript.

Acknowledgments

The authors wish to thank Hilaire Lam, Shu Hisata, and Kenji Mizumura, and the Weill Cornell Pathology Core, Core Laboratories Center, and Imaging Core Facility for technical assistance. This work was supported by the NIH grants R01 DK57661 and R01 HL079904 (to MEC); P01-HL114501 and R01-HL079904 (to AMKC); R01-HL133801 (to MEC and AMKC); and R00-HL125899 (to SMC).

Address correspondence to: Mary E. Choi, Division of Nephrology and Hypertension, Joan and Sanford I. Weill Department of Medicine, Weill Cornell Medical College, 525 East 68th Street, Box 3, New York, New York 10065, USA. Phone: 646.962.2605; Email: mechoi@med.cornell.edu. Or to: Augustine M.K.

Choi, Division of Pulmonary and Critical Care Medicine, Joan and Sanford I. Weill Department of Medicine, Weill Cornell Medical College, 525 East 68th Street, Box 83, New York, New York 10065, USA. Phone: 212.746.6005; Email: amc2056@med.cornell.edu.

1. US Department of Health and Human Services, Centers for Disease Control and Prevention, National Center for Health Statistics. *Health, United States, 2016: With Chartbook on Long-Term Trends in Health*. Hyattsville, Maryland, USA: National Center for Health Statistics; 2017. https://www.cdc.gov/nchs/data/hus/hus16.pdf. Accessed September 7, 2018.
2. Barnes PJ, Shapiro SD, Pauwels RA. Chronic obstructive pulmonary disease: molecular and cellular mechanisms. *Eur Respir J*. 2003;22(4):672–688.
3. Hogg JC, et al. The nature of small-airway obstruction in chronic obstructive pulmonary disease. *N Engl J Med*. 2004;350(26):2645–2653.
4. Mannino DM, Buist AS. Global burden of COPD: risk factors, prevalence, and future trends. *Lancet*. 2007;370(9589):765–773.
5. Decramer M, Janssens W, Miravitlles M. Chronic obstructive pulmonary disease. *Lancet*. 2012;379(9823):1341–1351.
6. Incalzi RA, et al. Chronic renal failure: a neglected comorbidity of COPD. *Chest*. 2010;137(4):831–837.
7. van Gestel YR, et al. Association between chronic obstructive pulmonary disease and chronic kidney disease in vascular surgery patients. *Nephrol Dial Transplant*. 2009;24(9):2763–2767.
8. Kidney Disease Statistics for the United States. The National Institute of Diabetes and Digestive and Kidney Diseases Health Information Center. NIH. https://www.niddk.nih.gov/health-information/health-statistics/kidney-disease. Accessed August 29, 2018.
9. Sandsmark DK, et al. Proteinuria, but not eGFR, predicts stroke risk in chronic kidney disease: Chronic Renal Insufficiency Cohort Study. *Stroke*. 2015;46(8):2075–2080.
10. Breyer MD, Susztak K. The next generation of therapeutics for chronic kidney disease. *Nat Rev Drug Discov*. 2016;15(8):568–588.
11. Akbari A, et al. Canadian Society of Nephrology commentary on the KDIGO clinical practice guideline for CKD evaluation and management. *Am J Kidney Dis*. 2015;65(2):177–205.
12. Polverino F, et al. A pilot study linking endothelial injury in lungs and kidneys in chronic obstructive pulmonary disease. *Am J Respir Crit Care Med*. 2017;195(11):1464–1476.
13. Yacoub R, et al. Association between smoking and chronic kidney disease: a case control study. *BMC Public Health*. 2010;10:731.
14. Ishizaka N, et al. Association between cigarette smoking and chronic kidney disease in Japanese men. *Hypertens Res*. 2008;31(3):485–492.
15. Agarwal R. Smoking, oxidative stress and inflammation: impact on resting energy expenditure in diabetic nephropathy. *BMC Nephrol*. 2005;6:13.
16. Sung RS, Althoen M, Howell TA, Ojo AO, Merion RM. Excess risk of renal allograft loss associated with cigarette smoking. *Transplantation*. 2001;71(12):1752–1757.
17. Ward MM, Studenski S. Clinical prognostic factors in lupus nephritis. The importance of hypertension and smoking. *Arch Intern Med*. 1992;152(10):2082–2088.
18. Jaimes EA, Tian RX, Raij L. Nicotine: the link between cigarette smoking and the progression of renal injury? *Am J Physiol Heart Circ Physiol*. 2007;292(1):H76–H82.
19. Orth SR, et al. Smoking as a risk factor for end-stage renal failure in men with primary renal disease. *Kidney Int*. 1998;54(3):926–931.
20. Salvatore SP, Troxell ML, Hecox D, Sperling KR, Seshan SV. Smoking-related glomerulopathy: expanding the morphologic spectrum. *Am J Nephrol*. 2015;41(1):66–72.
21. Nakahira K, Pabon Porras MA, Choi AM. Autophagy in pulmonary diseases. *Am J Respir Crit Care Med*. 2016;194(10):1196–1207.
22. Mizumura K, et al. Mitophagy-dependent necroptosis contributes to the pathogenesis of COPD. *J Clin Invest*. 2014;124(9):3987–4003.
23. Tuder RM, Petrache I. Pathogenesis of chronic obstructive pulmonary disease. *J Clin Invest*. 2012;122(8):2749–2755.
24. Bagdonas E, Raudoniute J, Bruzauskaite I, Aldonyte R. Novel aspects of pathogenesis and regeneration mechanisms in COPD. *Int J Chron Obstruct Pulmon Dis*. 2015;10:995–1013.
25. Mizushima N, Komatsu M. Autophagy: renovation of cells and tissues. *Cell*. 2011;147(4):728–741.
26. Choi AM, Ryter SW, Levine B. Autophagy in human health and disease. *N Engl J Med*. 2013;368(19):1845–1846.
27. Narendra D, Kane LA, Hauser DN, Fearnley IM, Youle RJ. p62/SQSTM1 is required for Parkin-induced mitochondrial clustering but not mitophagy; VDAC1 is dispensable for both. *Autophagy*. 2010;6(8):1090–1106.
28. Pabon MA, Ma KC, Choi AM. Autophagy and obesity-related lung disease. *Am J Respir Cell Mol Biol*. 2016;54(5):636–646.
29. Lam HC, et al. Histone deacetylase 6-mediated selective autophagy regulates COPD-associated cilia dysfunction. *J Clin Invest*. 2013;123(12):5212–5230.
30. Chen ZH, et al. Autophagy protein microtubule-associated protein 1 light chain-3B (LC3B) activates extrinsic apoptosis during cigarette smoke-induced emphysema. *Proc Natl Acad Sci USA*. 2010;107(44):18880–18885.
31. Chen ZH, et al. Egr-1 regulates autophagy in cigarette smoke-induced chronic obstructive pulmonary disease. *PLoS ONE*. 2008;3(10):e3316.
32. Ding Y, Kim Sl, Lee SY, Koo JK, Wang Z, Choi ME. Autophagy regulates TGF-β expression and suppresses kidney fibrosis induced by unilateral ureteral obstruction. *J Am Soc Nephrol*. 2014;25(12):2835–2846.
33. Hsiao HW, et al. The decline of autophagy contributes to proximal tubular dysfunction during sepsis. *Shock*. 2012;37(3):289–296.
34. Kitada M, Ogura Y, Monno I, Koya D. Regulating Autophagy as a therapeutic target for diabetic nephropathy. *Curr Diab Rep*. 2017;17(7):53.
35. Laucho-Contreras ME, Taylor KL, Mahadeva R, Boukedes SS, Owen CA. Automated measurement of pulmonary emphysema and small airway remodeling in cigarette smoke-exposed mice. *J Vis Exp*. 2015;(95):52236.
36. Mori K, et al. Endocytic delivery of lipocalin-siderophore-iron complex rescues the kidney from ischemia-reperfusion injury. *J Clin Invest*. 2005;115(3):610–621.

37. Zuo L, et al. Interrelated role of cigarette smoking, oxidative stress, and immune response in COPD and corresponding treatments. *Am J Physiol Lung Cell Mol Physiol*. 2014;307(3):L205–L218.
38. van der Vaart H, Postma DS, Timens W, ten Hacken NH. Acute effects of cigarette smoke on inflammation and oxidative stress: a review. *Thorax*. 2004;59(8):713–721.
39. Balaban RS, Nemoto S, Finkel T. Mitochondria, oxidants, and aging. *Cell*. 2005;120(4):483–495.
40. Cloonan SM, Choi AM. Mitochondria in lung disease. *J Clin Invest*. 2016;126(3):809–820.
41. Cherry AD, Piantadosi CA. Regulation of mitochondrial biogenesis and its intersection with inflammatory responses. *Antioxid Redox Signal*. 2015;22(12):965–976.
42. Ding Y, Kim Sl, Lee SY, Koo JK, Wang Z, Choi ME. Autophagy regulates TGF-β expression and suppresses kidney fibrosis induced by unilateral ureteral obstruction. *J Am Soc Nephrol*. 2014;25(12):2835–2846.
43. Filomeni G, Desideri E, Cardaci S, Rotilio G, Ciriolo MR. Under the ROS…thiol network is the principal suspect for autophagy commitment. *Autophagy*. 2010;6(7):999–1005.
44. Tait SW, Ichim G, Green DR. Die another way — non-apoptotic mechanisms of cell death. *J Cell Sci*. 2014;127(Pt 10):2135–2144.
45. Haspel J, et al. Characterization of macroautophagic flux in vivo using a leupeptin-based assay. *Autophagy*. 2011;7(6):629–642.
46. Kang R, Zeh HJ, Lotze MT, Tang D. The Beclin 1 network regulates autophagy and apoptosis. *Cell Death Differ*. 2011;18(4):571–580.
47. Molejon MI, Ropolo A, Re AL, Boggio V, Vaccaro MI. The VMP1-Beclin 1 interaction regulates autophagy induction. *Sci Rep*. 2013;3:1055.
48. Kim SI, Na HJ, Ding Y, Wang Z, Lee SJ, Choi ME. Autophagy promotes intracellular degradation of type I collagen induced by transforming growth factor (TGF)-β1. *J Biol Chem*. 2012;287(15):11677–11688.
49. Qu X, et al. Promotion of tumorigenesis by heterozygous disruption of the beclin 1 autophagy gene. *J Clin Invest*. 2003;112(12):1809–1820.
50. Pan B, Liu G, Jiang Z, Zheng D. Regulation of renal fibrosis by macrophage polarization. *Cell Physiol Biochem*. 2015;35(3):1062–1069.
51. Sica A, Mantovani A. Macrophage plasticity and polarization: in vivo veritas. *J Clin Invest*. 2012;122(3):787–795.
52. Clements M, et al. Differential Ly6C expression after renal ischemia-reperfusion identifies unique macrophage populations. *J Am Soc Nephrol*. 2016;27(1):159–170.
53. Wei Y, Chiang WC, Sumpter R, Mishra P, Levine B. Prohibitin 2 is an inner mitochondrial membrane mitophagy receptor. *Cell*. 2017;168(1-2):224–238.e10.
54. Kaushal GP, Shah SV. Autophagy in acute kidney injury. *Kidney Int*. 2016;89(4):779–791.
55. Ito S, et al. PARK2-mediated mitophagy is involved in regulation of HBEC senescence in COPD pathogenesis. *Autophagy*. 2015;11(3):547–559.
56. Lazarou M, et al. The ubiquitin kinase PINK1 recruits autophagy receptors to induce mitophagy. *Nature*. 2015;524(7565):309–314.
57. Bchir S, et al. Concomitant elevations of MMP-9, NGAL, proMMP-9/NGAL and neutrophil elastase in serum of smokers with chronic obstructive pulmonary disease. *J Cell Mol Med*. 2017;21(7):1280–1291.
58. Wang XR, et al. Increased serum levels of lipocalin-1 and -2 in patients with stable chronic obstructive pulmonary disease. *Int J Chron Obstruct Pulmon Dis*. 2014;9:543–549.
59. Eagan TM, et al. Neutrophil gelatinase-associated lipocalin: a biomarker in COPD. *Chest*. 2010;138(4):888–895.
60. Casanova C, et al. Microalbuminuria and hypoxemia in patients with chronic obstructive pulmonary disease. *Am J Respir Crit Care Med*. 2010;182(8):1004–1010.
61. Bulcun E, Ekici M, Ekici A, Kisa U. Microalbuminuria in chronic obstructive pulmonary disease. *COPD*. 2013;10(2):186–192.
62. Romundstad S, Naustdal T, Romundstad PR, Sorger H, Langhammer A. COPD and microalbuminuria: a 12-year follow-up study. *Eur Respir J*. 2014;43(4):1042–1050.
63. Polatli M, Cakir A, Cildag O, Bolaman AZ, Yenisey C, Yenicerioglu Y. Microalbuminuria, von Willebrand factor and fibrinogen levels as markers of the severity in COPD exacerbation. *J Thromb Thrombolysis*. 2008;26(2):97–102.
64. Chandra D, et al. The relationship between pulmonary emphysema and kidney function in smokers. *Chest*. 2012;142(3):655–662.
65. Pinto-Sietsma SJ, Mulder J, Janssen WM, Hillege HL, de Zeeuw D, de Jong PE. Smoking is related to albuminuria and abnormal renal function in nondiabetic persons. *Ann Intern Med*. 2000;133(8):585–591.
66. Sureshbabu A, Ryter SW, Choi ME. Oxidative stress and autophagy: crucial modulators of kidney injury. *Redox Biol*. 2015;4:208–214.
67. Jaimes EA, DeMaster EG, Tian RX, Raij L. Stable compounds of cigarette smoke induce endothelial superoxide anion production via NADPH oxidase activation. *Arterioscler Thromb Vasc Biol*. 2004;24(6):1031–1036.
68. van der Toorn M, et al. Cigarette smoke-induced blockade of the mitochondrial respiratory chain switches lung epithelial cell apoptosis into necrosis. *Am J Physiol Lung Cell Mol Physiol*. 2007;292(5):L1211–L1218.
69. Slebos DJ, et al. Mitochondrial localization and function of heme oxygenase-1 in cigarette smoke-induced cell death. *Am J Respir Cell Mol Biol*. 2007;36(4):409–417.
70. Naimi AI, et al. Altered mitochondrial regulation in quadriceps muscles of patients with COPD. *Clin Physiol Funct Imaging*. 2011;31(2):124–131.
71. D'Agostino B, et al. Exercise capacity and cytochrome oxidase activity in muscle mitochondria of COPD patients. *Respir Med*. 2010;104(1):83–90.
72. Puente-Maestu L, et al. Abnormal mitochondrial function in locomotor and respiratory muscles of COPD patients. *Eur Respir J*. 2009;33(5):1045–1052.
73. Komatsu M, et al. The selective autophagy substrate p62 activates the stress responsive transcription factor Nrf2 through inactivation of Keap1. *Nat Cell Biol*. 2010;12(3):213–223.
74. Li W, et al. FoxO1 promotes mitophagy in the podocytes of diabetic male mice via the PINK1/Parkin pathway. *Endocrinology*. 2017;158(7):2155–2167.
75. Zhao C, et al. Drp1-dependent mitophagy protects against cisplatin-induced apoptosis of renal tubular epithelial cells by improving mitochondrial function. *Oncotarget*. 2017;8(13):20988–21000.
76. Che R, Yuan Y, Huang S, Zhang A. Mitochondrial dysfunction in the pathophysiology of renal diseases. *Am J Physiol Renal Physiol*. 2014;306(4):F367–F378.

77. Choubey V, et al. BECN1 is involved in the initiation of mitophagy: it facilitates PARK2 translocation to mitochondria. *Autophagy*. 2014;10(6):1105–1119.
78. Lin F. Autophagy in renal tubular injury and repair. *Acta Physiol (Oxf)*. 2017;220(2):229–237.
79. Livingston MJ, Ding HF, Huang S, Hill JA, Yin XM, Dong Z. Persistent activation of autophagy in kidney tubular cells promotes renal interstitial fibrosis during unilateral ureteral obstruction. *Autophagy*. 2016;12(6):976–998.